Exchange coupling and helical spin order in the triangular lattice antiferromagnet $CuCrO_2$ using first principles*

Jiang Xue-Fan(江学范)[a)†], Liu Xian-Feng(刘先锋)[b)],
Wu Yin-Zhong(吴银忠)[a)], and Han Jiu-Rong(韩玖荣)[b)]

[a)] *Jiangsu Key Laboratory of Advanced Functional Materials, Changshu Institute of Technology, Changshu* 215500, *China*
[b)] *College of Physics Science and Technology, Yangzhou University, Yangzhou* 225002, *China*

(Received 5 November 2011; revised manuscript received 3 December 2011)

The magnetic and electronic properties of the geometrically frustrated triangular antiferromagnet $CuCrO_2$ are investigated by first principles through density functional theory calculations within the generalized gradient approximations (GGA)+U scheme. The spin exchange interactions up to the third nearest neighbours in the ab plane as well as the coupling between adjacent layers are calculated to examine the magnetism and spin frustration. It is found that $CuCrO_2$ has a natural two-dimensional characteristic of the magnetic interaction. Using Monte–Carlo simulation, we obtain the Néel temperature to be 29.9 K, which accords well with the experimental value of 24 K. Based on non-collinear magnetic structure calculations, we verify that the incommensurate spiral-spin structure with (110) spiral plane is believable for the magnetic ground state, which is consistent with the experimental observations. Due to intra-layer geometric spin frustration, parallel helical-spin chains arise along the a, b, or $a+b$ directions, each with a screw-rotation angle of about 120°. Our calculations of the density of states show that the spin frustration plays an important role in the change of d–p hybridization, while the spin-orbit coupling has a very limited influence on the electronic structure.

Keywords: magnetically ordered materials, multiferroic, spin frustration, spin orbit effects

PACS: 75.25.–j, 75.50.Ee, 71.15.–m, 71.70.Ej **DOI:** 10.1088/1674-1056/21/7/077502

1. Introduction

Triangular lattice antiferromagnets (TLAs) have received considerable attention in recent years due to their novel characteristics, such as exotic ground states, incommensurate spin structures and multiferroic properties.[1−3] Among them, the delafossite $CuCrO_2$ is of particular interest because of the discovery of its p-type transparent conducting property as an oxide[4] and magnetically driven ferroelectricity (FE).[5] The control of FE by a magnetic field is important for new spin-based device applications, and the flop of ferroelectric polarization by applying a magnetic field in $CuCrO_2$ has been observed.[6] Recently, the preparation and the properties of $CuCrO_2$[7] have attracted much attention, however, few theoretical studies[8] of the mechanism and origin of the novel characteristics mentioned above can be found in the literature.

$CuCrO_2$ with a delafossite structure has a symmetry of space group $R\bar{3}m$. The elements form triangular lattices stacking along the c-axis in the sequence Cu–O–Cr–O. As shown in Fig. 1, this structure consists of two-dimensional (2D) triangular-lattice CrO_2 layers of edge-sharing CrO_6 octahedra with Cr^{3+} ions ($S = 3/2$) separated by Cu^+ ions. An early neutron powder diffraction (NPD) study proposed that when below the Néel temperature (T_N) of 24 K, $CuCrO_2$ undergoes magnetic ordering into an out-of-plane 120° magnetic structure with the commensurate propagation vector along the (1/3, 1/3, 0) direction.[9] The more recent NPD study[10] suggested that two possible magnetic structures exist in $CuCrO_2$: one is the proper-screw spin structure, and the other is the cycloidal structure with the incommensurate propagation vector (0.329, 0.329, 0) below T_N. Polarized neutron-diffraction measurement on a single crystal revealed that the spiral plane is parallel to the (110) plane.[11]

*Project supported by the National Natural Science Foundation of China (Grant No. 10874021).
†Corresponding author. E-mail: xfjiang@cslg.edu.cn
© 2012 Chinese Physical Society and IOP Publishing Ltd

Previous theoretical analyses[5,12] have indicated that the inverse Dzyaloshinskii–Moriya (DM) mechanism[13] and the Katsura–Nagaosa–Balatsky (KNB) model[14] fail to explain the FE in $CuCrO_2$. Recent spin-polarized-neutron studies[11] supported that the electric polarization in $CuCrO_2$ can be explained by the theoretical prediction proposed by Arima.[15] In Arima's model, FE is induced by both the proper-screw magnetic structure and the d–p hybridization due to spin-orbit coupling (SOC) in a low-symmetry crystal. However, there are no further studies dealing with the origin of FE and the role of SOC in the d–p hybridization in $CuCrO_2$. Therefore, it is important to investigate the magnetic structure and check the role of SOC in $CuCrO_2$.

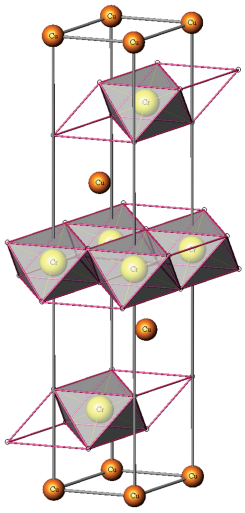


Fig. 1. (colour online) The crystal structure of $CuCrO_2$.

In this paper, we perform calculations based on both collinear and non-collinear magnetic structures using density functional theory (DFT). The magnetic structure, spin exchange interaction, and the effect of SOC on the electronic structure of $CuCrO_2$ are investigated in detail. The rest of the paper is organized as follows: in Section 2, we give the computational details; in Section 3, the spin exchange interactions, low temperature magnetic configuration, as well as the effect of SOC are discussed; and a brief conclusion is given at the end.

2. Computation methods

All calculations were performed using the projector augmented wave (PAW) method within DFT,[16] as implemented in the Vienna *ab initio* simulation package (VASP).[17] The exchange and the correlation effects were treated within the generalized gradient approximations (GGA).[18] To describe the strong electron correlation associated with the Cr 3d states, the on-site Coulomb energy U was taken into account in the GGA+U scheme. The values of U and J were assigned to 2.3 eV and 0.96 eV, respectively.[19,20]

In our calculations, two kinds of magnetic structures were considered, including both collinear and non-collinear spin systems. Convergences with respect to the plane-wave cutoff energy and k-point sampling were carefully checked. The plane wave cutoff energy was set to be 450 eV, and the convergence criterion for energy was taken as 10^{-4} eV. Brillouin zone integrations were performed with the tetrahedron method. A Monkhorst–Pack k-point mesh centred at Γ was generated with the density 8×8×2 grid for the collinear-spin system and 4×4×2 grid for the non-collinear-spin system.

3. Results and discussion

3.1. Spin exchange interactions

In order to understand the spin frustration and the magnetic properties of $CuCrO_2$, the magnetic interactions are estimated based on the collinear magnetic structure calculations. The spin exchange interactions up to the third nearest neighbours in the *ab* plane (see Fig. 2(a)), as well as the magnetic coupling between adjacent layers (J_c), are considered. For the collinear magnetic structures, we calculated five possible types of ordered spin states, which we tentatively named FM, AFM1, AFM2, AFM3, and AFM4 states for convenience of discussion. As shown in Fig. 2(b), the supercell has 72 atoms within 18 formula units. Because of the nature of the planar triangular lattice, it should be noted that the assumed AFM2, AFM3, and AFM4 states probably do not exist in nature at all. In these three states, when the interactions among the nearest-neighbour spins occur in their corresponding mechanisms, the arrangement of spins must be frustrated. Here we introduced the three states only for the purpose of estimating the spin-exchange interactions.

In the calculations, full optimizations of the lattice parameters are performed. Table 1 shows the re-

sults obtained within the GGA+U scheme. To estimate the spin exchange parameters J_1, J_2, J_3, and J_c, we map the relative energies of the five collinear ordered spin states (see Table 1) onto the corresponding energies given by the Heisenberg model $H = -\sum_{i,j} J_{ij} \boldsymbol{S}_i \cdot \boldsymbol{S}_j$,[21] where i, j are the site indices on a triangular lattice and J_{ij} denotes the spin-exchange interaction. The corresponding energy expressions for the $3 \times 2 \times 1$ supercells are given by

$$E_{\mathrm{FM}} = E_0 - 9(54J_1 + 54J_2 + 54J_3 + 54J_c)/4,$$
$$E_{\mathrm{AFM1}} = E_0 - 9(54J_1 + 54J_2 + 54J_3 - 18J_c)/4,$$
$$E_{\mathrm{AFM2}} = E_0 - 9(6J_1 - 18J_2 + 6J_3 + 22J_c)/4,$$
$$E_{\mathrm{AFM3}} = E_0 - 9(-18J_1 - 18J_2 + 54J_3 + 6J_c)/4,$$
$$E_{\mathrm{AFM4}} = E_0 - 9(-18J_1 + 6J_2 + 6J_3 + 6J_c)/4.$$

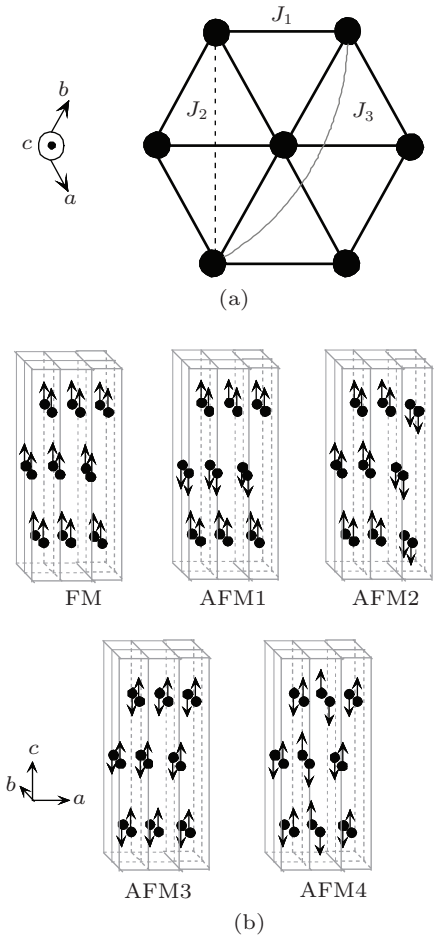


Fig. 2. (a) Illustration of the intra-layer spin exchange paths including the nearest-neighbour (J_1), the next-nearest neighbour (J_2), and the third-nearest neighbour (J_3) magnetic interactions. (b) Five ordered collinear-spin states of $CuCrO_2$. For simplicity, only the Cr^{3+} ions are shown. The spin-up and spin-down moments are represented by arrows.

We have calculated the exchange parameters, and the results are $J_1 = -2.972$ meV, $J_2 = 0.090$ meV, $J_3 = -0.163$ meV, $J_c = -0.069$ meV. The coupling J_1 describes a direct antiferromagnetic interaction between neighbouring Cr^{3+} ions within each layer, which is dominated by direct Cr–Cr d–d overlapping,[10] and the interlayer coupling J_c between adjacent Cr^{3+} planes is meditated by Cu^+ ions through the path Cr–O–Cu–O–Cr. From these calculated spin exchange parameters, we can see that couplings as represented by J_1 and J_3 are antiferromagnetic, which means that the spin frustration occurs in each triangle of J_1 and in each triangle of J_3, respectively. Furthermore, J_c is also antiferromagnetic, which means that spin frustration arises in each isosceles triangle made up of J_1 and J_c between adjacent Cr^{3+} layers. Due to the inter- and the intra-layer geometric spin frustrations, the helical-spin configuration of $CuCrO_2$ is preferred, which we will discuss in the next section.

Table 1. Experimental results and fully optimized crystal structure parameters (a and c), and values of energy (E) per formula unit and energy gap (E_g) for $CuCrO_2$ within different magnetic orderings using GGA+U calculations.

	a/Å	c/Å	E/eV	E_g/eV
Expt.	2.969[10]	17.138[10]	–	2.80[4]
FM	2.999	17.311	–27.8968	1.07
AFM1	3.000	17.318	–27.8974	1.17
AFM2	2.997	17.304	–27.9151	1.20
AFM3	2.996	17.298	–27.9231	1.28
AFM4	2.996	17.297	–27.9244	1.30
TAFM	2.993	17.278	–28.0642	1.48

Since the interlayer Cr–Cr spacing ($\sim$ 5.7 Å) is much larger than the intra-layer one ($\sim$ 3.0 Å), the system may show a quasi-2D manner. Our calculated ratio $J_c/J_1 \approx 0.02$ has confirmed this conjecture well and is also consistent with the 2D character of the electronic structure.[22] Comparing with $AgCrO_2$, which belongs to the TLA family too, the ratio $J_c/J_1 \approx 1.64$,[19] which implies that $CuCrO_2$ has a more pronounced 2D character than $AgCrO_2$. Thus, $CuCrO_2$ is a typical example of the 2D triangular lattice Heisenberg antiferromagnet (TLHAF).

Furthermore, we estimate the Néel temperature by using Monte–Carlo simulation. A classical three-dimensional (3D) Heisenberg antiferromagnet with weak interlayer interaction is employed to simulate the magnetic behaviour of $CuCrO_2$. Due to the weak interlayer interactions, we define the chirality of spins for each elementary triangle within each layer as the

order parameter of the present system[23]

$$\boldsymbol{\kappa}_{\boldsymbol{r}} = \frac{2}{3\sqrt{3}}(\boldsymbol{S_1} \times \boldsymbol{S_2} + \boldsymbol{S_2} \times \boldsymbol{S_3} + \boldsymbol{S_3} \times \boldsymbol{S_1}),$$

and $\boldsymbol{\kappa} = \langle \boldsymbol{\kappa}_{\boldsymbol{r}} \rangle$, where 1, 2, and 3 are the corner sites of the elementary cell centred at the dual-lattice vector $\boldsymbol{r}$, and $\langle \cdots \rangle$ denotes the averaged value on a 36×36×6 lattice with periodical boundary condition. The susceptibility associated with staggered chirality has been defined in Ref. [21] as

$$\chi_{\boldsymbol{\kappa}} = \langle \boldsymbol{\kappa}^2 \rangle - \langle \boldsymbol{\kappa} \rangle^2.$$

Typically, the first 2000 Monte–Carlo simulations (MCSs) allow the system to reach its equilibrium state, and the statistical process is done during the next 40000 MCSs. Our numerical results are shown in Fig. 3, and the Néel temperature of the system can be approximately taken as the phase temperature related to the chirality. From Fig. 3, one can obtain $k_{\rm B}T_{\rm N}/J_1 = 0.87$, i.e., $T_{\rm N} = 29.9$ K, which accords well with the experimentally observed value of 24 K.[19]

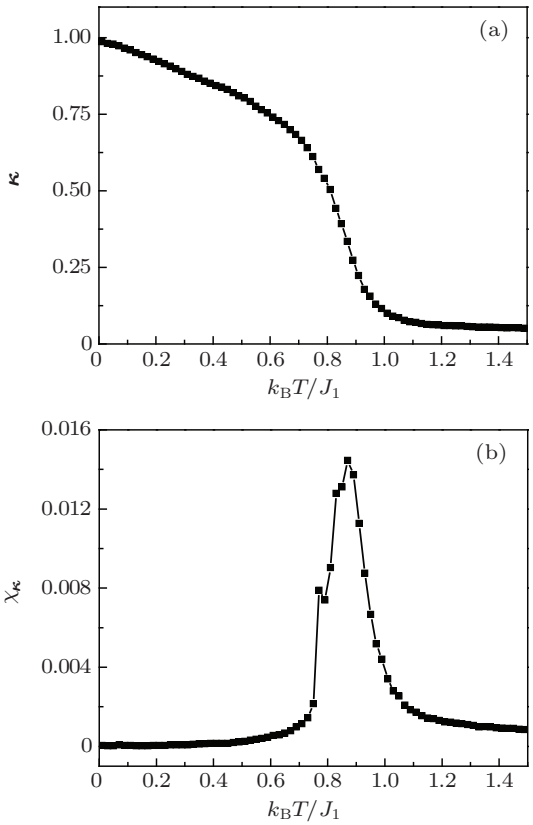


Fig. 3. Staggered (a) chirality and (b) chiral susceptibility, each as a function of temperature.

3.2. Helical-spin order

The early NPD study[19] showed that $CuCrO_2$ has a simple commensurate magnetic modulation vector $\boldsymbol{q} = (1/3, 1/3, 0)$. From symmetry analysis, Seki *et al.*[5] pointed out that only two possible spin configurations exists for the out-of-plane 120° spin structure in terms of the direction of the spiral plane parallel to the (110) or (1$\bar{1}$0) plane. Moreover, the electric polarization measurement determined the ground state structure to be the spin configuration with the (110) spiral plane.[11] The recent NPD measurement indicated an incommensurate spiral-spin structure with an in-plane wave vector $\boldsymbol{q} = (0.329, 0.329, 0)$ below $T_{\rm N}$,[10] corresponding to the 118° spin structure. More recent XRD measurements revealed that a slightly distorted triangular lattice appears in the ground state.[24] For simplicity, we consider the triangular antiferromagnetic (TAFM) state to be 120° spin configuration with the (110) spiral plane, and the slight lattice distortion is negligible. The TAFM state is chosen as the initial magnetic structure here. Non-collinear magnetic structure calculations have been performed thereafter on a 3×3×1 supercell of 108 atoms with 27 formula units.

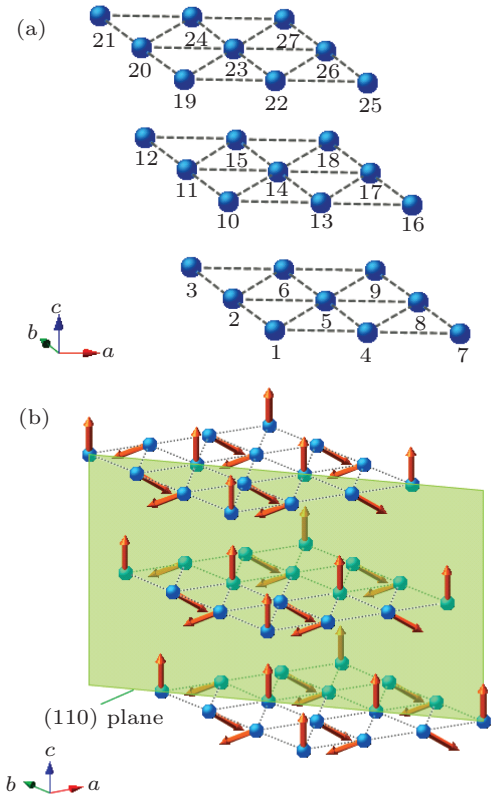


Fig. 4. (colour online) The detailed magnetic structure of $CuCrO_2$: (a) 27 Cr^{3+} ions at the different sites in the 3×3×1 supercell; and (b) plot of spin order within the TAFM state with the spin spiral plane parallel to the (110) plane. For simplicity, only the Cr^{3+} ions are shown. The arrow denotes the direction of the magnetic moment.

From Table 1, firstly it is clear that our theoretical values $a = 2.993$ Å and $c = 17.278$ Å in the TAFM state are consistent with the experimental values. Secondly, the TAFM state has a much lower total energy than the other states, which indicates that TAFM spin configuration may be the best choice for the ground state. Moreover, from Table 1, one can see that the energy gaps increase from 1.07 eV for FM to 1.48 eV for TAFM, and the band gap for TAFM is closer to the experimental value 2.8 eV.[4] So the TAFM state should be more suitable for the spin arrangement of Cr ions in $CuCrO_2$.

Table 2. The calculated magnetic moments of Cr^{3+} in $CuCrO_2$ in the TAFM state.

Cr	mag_x	mag_y	mag_z	mag_total
1	0.000	-0.007	2.881	2.881
2	–1.225	2.156	–1.470	2.883
3	1.230	–2.160	–1.460	2.883
4	–1.222	2.158	–1.469	2.882
5	1.234	–2.186	–1.419	2.884
6	–0.010	–0.004	2.884	2.884
7	1.227	–2.167	–1.452	2.883
8	0.006	–0.012	2.884	2.884
9	–1.242	2.183	–1.417	2.884
10	–0.003	0.001	2.878	2.878
11	–1.229	2.159	–1.458	2.881
12	1.224	–2.168	–1.445	2.879
13	–1.230	2.176	–1.431	2.880
14	1.226	–2.170	–1.449	2.883
15	0.010	–0.012	2.881	2.881
16	1.223	–2.164	–1.450	2.878
17	–0.010	0.008	2.880	2.880
18	–1.235	2.167	–1.437	2.879
19	–0.007	0.003	2.878	2.878
20	–1.232	2.172	–1.436	2.881
21	1.217	–2.174	–1.441	2.878
22	–1.229	2.157	–1.461	2.881
23	1.220	–2.173	–1.449	2.883
24	–0.011	–0.003	2.880	2.880
25	1.227	–2.172	–1.437	2.879
26	0.001	–0.017	2.881	2.881
27	–1.239	2.165	–1.435	2.878

We give the calculated magnetic moments of Cr^{3+} at the different sites (see Fig. 4(a)) for the TAFM state in Table 2, and the detailed magnetic structure of the TAFM is plotted in Fig. 4(b). Within the TAFM configuration, all magnetic moments lie in the spin spiral plane, which is parallel to the (110) plane, and is normal to the triangular lattice plane. Our calculated results indicate that $CuCrO_2$ has an incommensurate spiral-spin structure, which is in good agreement with the experimental observations.[10] None of the calculated angles of each three neighbouring spins are strictly 120°. Actually, they can vary from 118° to 121°. In this out-of-plane magnetic structure, the helical-spin chains run along the a direction, and they repeat along the b direction while advancing the screw-rotation anticlockwise by about 120°. Along each helical-spin chain, spins emerge with an anticlockwise rotation of nearly 120°. Considering the trigonal symmetry of $CuCrO_2$, the b direction and the $a + b$ direction are equivalent to the a direction. Therefore, helical-spin chains with about 120° screw-rotation are also found along the b and the $a + b$ directions in our calculations.

3.3. Effect of spin-orbit coupling

To consider the effect of the SOC of $CuCrO_2$ in the TAFM spin state, we carried out GGA+U and GGA+U+SOC calculations. The calculated total energy per formula unit is -28.067 eV without consideration of the SOC. When the SOC is turned on, the energy decreases to -28.075 eV. This indicates that the SOC favours the stabilization of the non-collinear-spin ground state.

The orbital-resolved densities of states (DOSs) obtained for collinear magnetic structure AFM4 and non-collinear magnetic structure TAFM are shown in Fig. 5, respectively. Due to the performance of the non-collinear magnetic structure calculations, here, we cannot distinguish the DOS between the spin-up and spin-down states. Within the GGA+U scheme, near the Fermi level, the conduction band and the interval from -1.5 to 0 eV in the valence band are both dominated mainly by Cr 3d states. The lower part of the spectrum between -8 and -3 eV in the valence band is occupied mainly by O 2p states. The upside of the valence band with an interval from -3 to -1.0 eV consists mostly of Cu 3d states. Cu can be assigned to a monovalent d^{10} configuration, which is consistent with the experimental observations.[4,22]

In order to consider the effect of spin frustration in $CuCrO_2$, the electronic structures are compared between the AFM4 and TAFM states. The DOSs of the two systems are both obtained within the GGA+U scheme, as shown in Fig. 5. Compared with the results of the AFM4 state, the energy gap of the TAFM state increases by 0.18 eV, and the DOSs of the Cu 3d,

Cr 3d, and O 2p bands become much more localized in the valence bands due to the strong spin frustration of the magnetic ions. Moreover, one can see that apparent changes of the DOS distribution occur in the conduction bands. As a result, the hybridization between Cr 3d and O 2p also varies correspondingly due to the spin frustration. Figures 5(b) and 5(c) show the DOSs of the TAFM state with and without consideration of the SOC, respectively. When the SOC is turned on, the DOS distribution and the hybridization between Cr 3d and O 2p also vary, although the discrepancy is rather small. Furthermore, it is found that the bond lengths of Cr–O and Cu–O change $\sim 10^{-4}$ Å. Simultaneously, the bond angles of Cr–O–Cr and Cu–O–Cu change $\sim 0.02°$. All these findings indicate that the SOC has a weak influence on the electronic structure. Therefore, we conclude that both the spin frustration and the SOC can modify the hybridization of electronic orbits in such a way that the charge centre shifts, and that the spin frustration is more responsible for the change in the d–p hybridization in $CuCrO_2$.

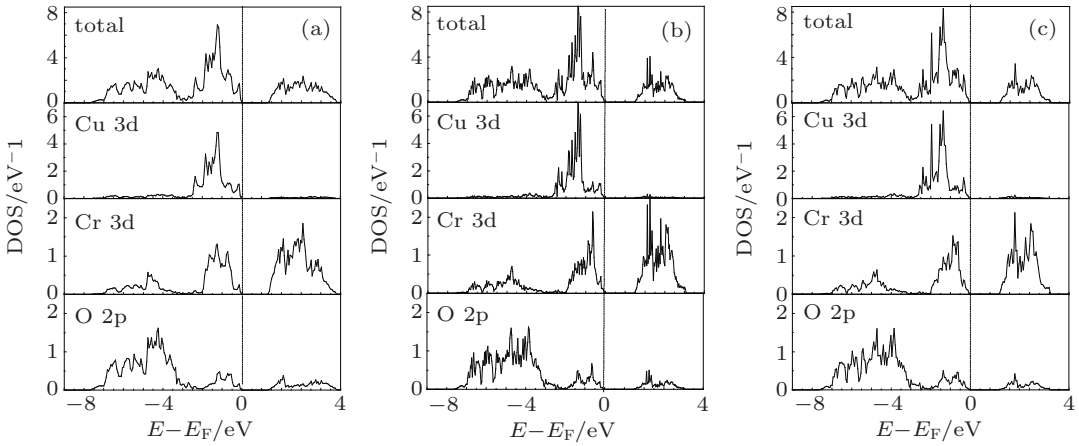


Fig. 5. (colour online) Total and orbit-resolved DOSs per formula unit of $CuCrO_2$ in the AFM4 and TAFM spin configurations: (a) the DOS of the AFM4 state, (b) the DOS of the TAFM state within the GGA+U scheme, and (c) the DOS of the TAFM state within the GGA+U+SOC scheme. The Fermi level corresponds to 0.0 eV.

4. Conclusion

In this paper, we calculate the GGA+U electronic structures of the different magnetic configurations of $CuCrO_2$. Our calculations show that the triangular frustrated spin configuration is most suitable for the magnetic ground state. $CuCrO_2$ has an incommensurate magnetic structure with proper-screw spin ordering. Due to the intralayer geometric spin frustration, helical-spin chains emerge with the screw-rotation angle at nearly 120°. The calculated results of the magnetic interactions show that $CuCrO_2$ is a typical example of the 2D TLHAF. The Néel temperature is calculated to be 29.9 K using the Monte–Carlo simulation, which accords well with the experimentally observed value of 24 K. The calculation results of the electronic structure show that the spin frustration has a stronger effect on changing the d–p hybridization in $CuCrO_2$ than SOC.

References

[1] Collins M F and Petrenko O A 1997 *Can. J. Phys.* **75** 605
[2] Ye F, Fernandez-Baca J A, Fishman R S, Ren Y, Kang H J, Oiu Y and Kimura T 2007 *Phys. Rev. Lett.* **99** 157201
[3] Hemmida M, Krug von Nidda H-A, Büttgen N, Loidl A, Alexander L K, Nath R, Mahajan A V, Berger R F, Cava R J, Singh Y and Johnston D C 2009 *Phys. Rev.* B **80** 054406
[4] Arnold T, Payne D J, Bourlange A, Hu J P, Egdell R G, Piper L F J, Colakerol L, De Masi A, Glans P-A, Learmonth T, Smith K E, Guo J, Scanlon D O, Walsh A, Morgan B J and Watson G W 2009 *Phys. Rev.* B **79** 075102
[5] Seki S, Onose Y and Tokura Y 2008 *Phys. Rev. Lett.* **101** 067204
[6] Kimura K, Nakamura H, Kimura S, Hagiwara M and Kimura T 2009 *Phys. Rev. Lett.* **103** 107201
[7] Scanlon D O and Watson G W 2011 *J. Mater. Chem.* **21** 3655
[8] Poienar M, Damay F and Martin C 2010 *Phys. Rev.* B **81** 104411
[9] Kadowaki H, Kikuchi H and Ajiro Y 1990 *J. Phys.*: *Condens. Matter* **2** 4485
[10] Poienar M, Damay F, Martin C, Hardy V, Maignan A and André G 2009 *Phys. Rev.* B **79** 014412

[11] Soda M, Kimura K, Kimura T, Matsuura M and Hirota K 2009 *J. Phys. Soc. Jpn.* **78** 124703
[12] Kimura K, Nakamura H, Ohgushi K and Kimura T 2008 *Phys. Rev.* B **78** 140401 (R)
[13] Sergienko I A and Dagotto E 2006 *Phys. Rev.* B **73** 094434
[14] Katsura H, Nagaosa N and Balatsky A V 2005 *Phys. Rev. Lett.* **95** 057205
[15] Arima T 2007 *J. Phys. Soc. Jpn.* **76** 073702
[16] Kresse G and Joubert D 1999 *Phys. Rev.* B **59** 1758
[17] Kresse G and Furthmüller J 1996 *Phys. Rev.* B **54** 11169
[18] Perdew J P, Burke K and Ernzerhof M 1996 *Phys. Rev. Lett.* **77** 3865
[19] Kan E J, Xiang H J, Zhang Y, Lee C and Whangbo M-H 2009 *Phys. Rev.* B **80** 104417
[20] Mazin I I 2007 *Phys. Rev.* B **75** 094407
[21] Zagoulaev S and Tupitsyn I I 1997 *Phys. Rev.* B **55** 13528
[22] Maignan A, Martin C, Frésard R, Eyert V, Guilmeau E, Hébert S, Poienar M and Pelloquin D 2009 *Solid State Commun.* **149** 962
[23] Capriotti L, Cuccoli A, Tognetti V and Vaia R 1999 *J. Appl. Phys.* **85** 6073; Capriotti L, Vaia R, Cuccoli A and Tognetti V 1998 *Phys. Rev.* B **58** 273
[24] Kimura K, Otani T, Nakamura H, Wakabayashi Y and Kimura T 2009 *J. Phys. Soc. Jpn.* **78** 113710